Seasonally Modulated Tropical Drought Induced by Volcanic Aerosol

RENU JOSEPH

Department of Atmospheric and Oceanic Science, University of Maryland, College Park, College Park, Maryland

NING ZENG

Department of Atmospheric and Oceanic Science, and Earth System Science Interdisciplinary Center, University of Maryland, College Park, College Park, Maryland

(Manuscript received 1 April 2009, in final form 30 September 2009)

ABSTRACT

Major volcanic events with a high loading of stratospheric aerosol have long been known to cause cooling, but their impact on precipitation has only recently been emphasized, especially as an analog for potential geoengineering of climate. Here, the authors use a coupled atmosphere–ocean–land–vegetation model in conjunction with observations to study the effects of volcanic aerosol on the tropical and subtropical precipitation. The small internal variability in the model enables a clear identification of the volcanic impact, which is broadly supported by observations, especially for the large Pinatubo event. Area averaged rainfall over land between 40°S and 40°N decreases by about 0.15 mm day^{-1}, 4–5 months after the height of a major volcanic aerosol loading, such as from Pinatubo, with regional changes as large as 0.6 mm day^{-1} or higher, such as over the Amazon and equatorial Africa. These anomalies migrate seasonally, following the movement of monsoon rainfall. This is because the low heat capacity of the land leads to rapid response of rainfall there, owing to the energy imbalance caused by volcanic aerosol cooling. In contrast, precipitation response over the ocean is much slower and considerably damped because of the much larger heat capacity. In addition, the difference in heat capacities over land and over ocean leads to an anomalous land–sea thermal contrast, which could further contribute to the reduction of rainfall over land. The volcano-induced drought may have significant impact on the ecosystem, agriculture, and the carbon cycle, especially in the monsoon regions.

1. Introduction

The cooling effect of volcanoes that injects particles and gases into the stratosphere has been long known. The earliest records of surface cooling from such events stems from Franklin (1784), who attributed the unusually cool summer of 1783 to the Laki volcano that erupted in Iceland that year. More recent modeling and observational studies have confirmed that there can be substantial effects of volcanic eruptions on surface temperature (e.g., Humphreys 1940; Hansen et al. 1992; Minnis et al. 1993; Robock and Mao 1995; Robock 2000 and references therein; Jones et al. 2003; Wigley 2000; Free and Angell 2002). This cooling is affected by the injection of sulfuric gas into the stratosphere, which combines with water and oxygen to form small optically important particles that get redistributed producing a veil of aerosol that blocks incoming solar radiation to the earth. Further, the aerosols of low-latitude volcanoes cover the tropics fairly quickly and uniformly, while the aerosols of high-latitude volcanoes normally are confined to the extratropics. It is worth noting that the three eruptions with the largest aerosol loadings (Agung, 1963; El Chichón 1982; Pinatubo, 1991) in the latter half of the twentieth century all occurred at very low latitudes. These are the events studied in this paper.

Compared to this well-known cooling effect, fewer studies have examined the impact of the volcanic aerosols on the hydrologic cycle. The higher variability of precipitation in comparison with temperature makes it more challenging to diagnose the impact of volcanoes on precipitation. One of the first studies to address the precipitation response to volcanic events was Robock and Liu (1994). They used the Goddard Institute for Space Studies

Corresponding author address: Ning Zeng, Department of Atmospheric and Oceanic Science, University of Maryland, College Park, College Park, MD 20742-2425.
E-mail: zeng@atmos.umd.edu

DOI: 10.1175/2009JCLI3170.1

general circulation model (GCM) to analyze the precipitation response to major volcanoes and noted a reduced tropical precipitation for 1–2 years following the volcanic signal. Oman et al. (2005) used Nile River records to indicate the impact of high-latitude volcanoes on the African monsoon. Trenberth and Dai (2007) used observations of global freshwater discharge and total continental precipitation to indicate a 0.07 Sv (1 Sv $\equiv 10^6$ m^3 s^{-1}) decrease during the 1-yr period following the Pinatubo eruption. They also presented the spatial pattern of precipitation decrease and the Palmer Drought Severity Index for the 12-month average following the Pinatubo event. Gu et al. (2007) while identifying the interannual and longer-time variability in precipitation using the Global Precipitation Climatology Product (GPCP) data quantified the decrease of the tropical mean precipitation due to the Pinatubo and El Chichón eruptions. The water vapor responses to the major volcanic events have been discussed by Soden et al. (2002). They examined the total column water vapor from the National Aeronautics and Space Administration (NASA) water vapor product along with model results and found a decrease in total column water vapor of about 3% in both the model and observations during the peak of Pinatubo cooling.

In addition, some studies have also examined the relationship of changes in radiative forcing and precipitation. Wild et al. (2008) used observations to connect changes in net reduction in shortwave (SW) radiation to changes in precipitation. Using idealized GCM experiments, Yang et al. (2003) show that the response of precipitation to radiative changes in the atmosphere depends on both the radiative changes as well as the changes in surface warming. Lambert and Allen (2009) analyze changes in precipitation for the whole globe, ocean, and land in several GCMs. They indicate precipitation changes over the oceans can be expressed as an energy balance between the direct and surface temperature–dependent effects of external climate forcings. However, precipitation over land is more complicated.

Recent interest in the possible use of sulfate aerosols injected directly into the stratosphere to reduce incoming solar radiation, as a geoengineering technique, to combat the effects of global warming, have generated considerable discussion in literature with respect to potential impacts on the hydrologic cycle. Several idealized studies have examined, to varying extents, the reduction of incoming shortwave radiation due to sulfate aerosols. Results indicate that these processes not only cool the surface but also affect the precipitation, especially in the tropics (e.g., Robock et al. 2008; Rasch et al. 2008; Bala et al. 2008).

A good analog for understanding the impact of aerosol geoengineering is the volcanic aerosol effect. However, there have been very few studies on the hydrologic cycle response to volcanic aerosol (primarily, Robock and Liu 1994; Trenberth and Dai 2007). These studies all suggest a reduction in tropical precipitation under additional stratospheric aerosol loading. We reason that because tropical precipitation has strong seasonal movement, following the seasonal movement of the sun, an anomalous perturbation to the solar energy incident on the surface should also have a seasonal dependence. Because of the large difference in the heat capacity of land and ocean, we also expect a different response to volcanic forcing between land and ocean. In this paper, we discuss the effect of volcanic aerosols on hydrologic processes, focusing on the tropical and subtropical land regions where agriculture strongly depends on the seasonal migration of monsoon rainfall. We use a coupled atmosphere–ocean–land–vegetation model in conjunction with observations to study the seasonal evolution of precipitation anomalies in response to volcanic aerosol forcing and develop an understanding of the underlying mechanisms. Using seasonal composites of precipitation response we examine the regions where precipitation has decreased in observations and our model. We further examine the potential of land–sea contrast to explain the seasonal decreases of precipitation. Lastly, as volcanic cooling is known to affect the carbon uptake by the land–vegetation system (Gu et al. 2002; Jones and Cox 2001), we analyze the impact of the reduction in temperature and precipitation on the vegetation and carbon cycle in a coupled climate model.

2. Brief description of the model and data

a. Model description

The model is a coupled atmosphere–ocean–land–vegetation model of intermediate complexity. Different versions of this model have been used in several climate studies in evaluating the West African monsoon, Indian monsoon, and the Asian–Australian monsoon as part of the Climate of the Twentieth Century (C20C) project (Scaife et al. 2008; Kucharski et al. 2008; Zhou et al. 2008). The model is also part of the Coupled Carbon Cycle Climate Model Intercomparison Project (C4MIP; Zeng et al. 2004; Friedlingstein et al. 2006; Qian et al. 2010). The land and vegetation components have also been used to study the impact of climate variability such as the El Niño–Southern Oscillation (ENSO) on vegetation and the carbon cycle (Zeng et al. 2005; Qian et al. 2008).

The model consists of the global version of the atmospheric model Quasi-equilibrium Tropical Circulation Model (QTCM) (Neelin and Zeng 2000; Zeng et al. 2000), which simulates a reasonable seasonal climate compared to observations in the tropics and midlatitudes.

TABLE 1. Details of the three major volcanic events in the latter half of the twentieth century: Eruption date, location, month of maximum optical depth, and the periods used in this study are shown here.

Volcanic event	Eruption time	Location of eruption	Month of maximum optical depth	1-yr period of maximum response used in analysis	JFM period	JAS period
Pinatubo	June 1991	Philippines	Nov 1991	Oct 1991/Sep 1992	1992	1992
El Chichón	Mar 1982	Mexico	Aug 1982	Jul 1982/Jun 1983	1983	1982
Agung	Feb 1963	Indonesia	Aug 1963	Jul 1963/Jun 1964	1964	1963

The QTCM is coupled to the simple-land model (Zeng et al. 2000), and a slab mixed layer ocean model with Q-flux to represent the effects of ocean dynamics (Hansen et al. 1983). The mixed layer ocean depth used here is the annual mean derived from Levitus et al. (2000). The terrestrial carbon model Vegetation–Global–Atmosphere–Soil (Zeng 2003; Qian et al. 2008) is a dynamic vegetation model with full soil carbon dynamics but without the albedo feedback of vegetation.

The model response is examined as an ensemble average of 9 members, thereby reducing the fluctuations due to natural variability. All model results presented in this paper will be ensemble averages of the appropriate quantities. The individual members were forced with differing initial conditions. Though the model was run from 1870 to 2005, we focus our analyses only on 1960–2000, to facilitate comparison with observations. The model was forced by observed CO_2, sulfate aerosols from Koch et al. (1999), volcanic aerosol (Amman et al. 2003), and solar forcing (Crowley 2000). Specifically, all volcanic aerosols are assumed to be well mixed and are applied uniformly in the zonal dimension; they change only in the meridional direction. Each tropical eruption, the aerosol cloud originates in the tropics, builds and spreads over a few months before decaying and is transported poleward six months to a year after the eruption as in Amman et al. (2003). Because of the low vertical resolution in the climate model, which uses a Galerkin framework in the vertical, the optical thickness of the aerosol is converted to a reduction in shortwave radiation at the top of the atmosphere. An example of the rate of distribution of the aerosol, the optical depth is shown in section 3. The model has a climate sensitivity of about 3 K in global mean surface air temperature at doubled CO_2.

b. Data

The observational data used to validate the precipitation and surface air temperature (SAT) response to volcanic events is the Climatic Research Unit (CRU) precipitation and temperature data (Mitchell et al. 2004) and the GPCP precipitation data (Adler et al. 2003; Huffman et al. 1997) over land. The sea surface temperature (SST) reference dataset is the Hadley Center's sea ice and SST analysis (HadISST data) (Rayner et al. 2003).

c. Methodology

The timing of the three volcanic events (see Table 1) in this study is such that they all happened during periods when the El Niño also occurred. Therefore, while examining the associated climate response to volcanic events in observations, the natural variability associated with ENSO has to be removed. The method used to remove ENSO is similar to the method used by Chen et al. (2008), the details of which can be found in the appendix. The idea behind the method is that ENSO responses occur with different lags globally due to atmospheric teleconnections. In lieu of removing contemporaneous correlations only, we remove the response of ENSO corresponding to the lagged regression explaining the largest percentage of variance within a 12-month window. Though this technique does not remove the nonstationary components of ENSO (Compo and Sardeshmukh 2010; Penland and Matrosova 2006), it does remove the response due to the maximum stationary signal of ENSO at each point. The model uses a mixed layer ocean so there is no internally generated ENSO variability.

3. Results

The optical thickness of volcanic aerosols averaged between 40°S and 40°N used as a forcing in our model is shown in the top panel of Fig. 1. There are three large volcanic events during the period 1960–2000 with optical depth greater than a 0.06 threshold: Agung, El Chichón, and Pinatubo (see Table 1), with Pinatubo having a maximum area averaged forcing of about 0.25. The remaining panels show the overall temperature and precipitation response in the model as compared to observations. In accordance with the increase in optical depth, and hence the decreased shortwave radiation absorbed during major volcanic events, the model responds with a greater reduction in anomalous SAT and precipitation, with the response to Pinatubo event being the largest. It is encouraging to note that the precipitation response over land in the model is similar to the regressed precipitation plot obtained by Gu et al. (2007, Fig. 8c) for the GPCP precipitation data corresponding to volcanic forcing. Even the small increase below the 0.06 threshold in the optical

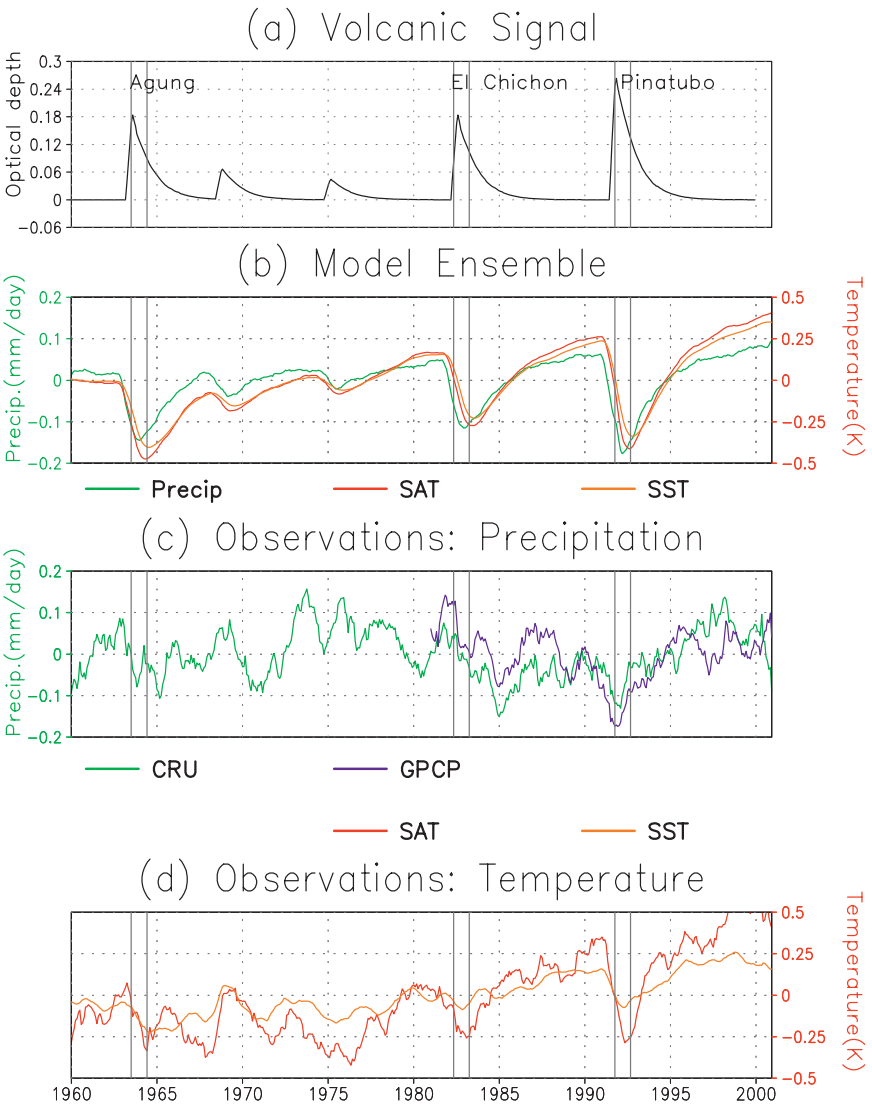

FIG. 1. Time series of precipitation and temperature in the model and observations in relation to the major volcanic events averaged between 40°N and 40°S. (a) The optical depth of the stratospheric aerosols used as a forcing in the model. (b) Model results for land precipitation (green, mm day^{-1}), land air temperature (red, K), and SST (orange, K). (c) Terrestrial precipitation for the CRU (green) and GPCP (purple) observations (mm day^{-1}). (d) SAT from CRU observations (red, K) and SST from HADISSTs (orange, K) are shown. In panels (b)–(d), all results presented as anomalies smoothed with a 12-month running mean. Anomalies are calculated from climatologies for the length of the data shown. For observations, the effects of ENSO were regressed out using the Niño-3.4 index as described in the text.

depth produces corresponding changes in SAT, SST, and precipitation in the model. These events, however, are too small to have any reasonable signal in observations (Figs. 1c and 1d). Even the largest volcanic signal cannot be unequivocally identified in the precipitation observations owing to the higher variability of the coupled nature of the earth–atmosphere system. The use of a mixed layer model leads to smaller variability on interannual to interdecadal time scales, thus a clearer signal in response to the external volcanic forcing.

In analyzing observations, the ENSO-related variability has been removed as discussed in the methodology section. Despite the removal of ENSO variability, large variabilities still remain, both in GPCP and CRU. The reduction of precipitation during the Pinatubo period is the strongest and the magnitude of reduction (about

0.15 mm day^{-1}) in the model is comparable to that in the GPCP data. The higher variability in the precipitation data compounded with the lack of reliable data the further one goes back in time precludes detailed analysis of volcanic events earlier than those highlighted in this paper (Trenberth and Dai 2007). Both the SAT and SST observations show a significant trend of about 0.5 K. However, the temperature decrease of about 0.35 K can be seen for all three volcanic events in the SAT for the model and observations. The temperature response of the model shows a larger decrease in the tropics over land than over ocean because of the lower heat capacity of the land. This is in accordance with observations shown in the bottom panel of Fig. 1.

With the intent of examining the composites of the annual and the seasonal response to the volcanic aerosol forcing, we chose the year of maximum response to be 1 month prior to and 11 months after the maximum of the optical depth. This period was chosen so as to include the months of maximum response of the austral and boreal summer (i.e., January and July). The period of maximum annual response thus defined is shown by the gray lines in Fig. 1 and are also indicated in Table 1. The period representative of the summer and winter season used in the analysis are shown in the table. Though the three volcanic events originated in different months during the year and had different intensities as reflected in the differences in optical depth (Fig. 1a), the model response of precipitation is intrinsically locked to the seasonal cycle as discussed later. Hence, to illustrate the overall response of volcanoes during summer and winter, composites are made using the time periods indicated in Table 1. This approach has also been used by Schneider et al. (2009) in their evaluation of the volcanic effects in the Community Climate System Model.

For all the results in the remaining text, the effect of the trend seen in Fig. 1 was initially removed. Then, as discussed in the methodology, the effect of ENSO has been removed before the composite response to the three volcanic events was made. The top panels of Fig. 2 are the 1-yr composites of the three volcanoes for the period of maximum volcanic response indicated in Table 1, in the model and in the CRU observations. The model response clearly shows a decrease in precipitation over equatorial Africa, the northern part of South America, northern Australia, and the Indian subcontinent. There are regional differences between observations and the model in the tropics in the African and the South American continent. The decrease in precipitation in the observations is less organized and patchier than in the model. However, when averaged over the large region of 40°S–40°N, they have comparable precipitation decrease of about 0.15 mm day^{-1} (Fig. 1). The three-volcano composite in the observations is dominated by the results of Pinatubo because it was a stronger event and had the most reliable data, while the results from the model are similar to each other since the model inherently has less variability. The 1-yr average of observational composite in Fig. 2 is similar to Fig. 3a of precipitation anomalies of Trenberth and Dai (2007).

A seasonal shift in the precipitation response is seen when the spatial plots of the austral and boreal summer plots are examined (middle and bottom panels of Fig. 2). In the austral summer [January–March (JFM)], there is a decrease in precipitation over South Africa, northern Australia, and South America, both in observations and in the model. These are regions dominated by monsoonal flows in this season. This decrease shows up consistently in the three individual events in both observations and in the model (individual figures not shown). However, in observations, the decrease in precipitation extends farther south in Africa than in the model. This is because of a bias in the model climatology of the Kalahari Desert, which spans a larger area than reality. In the boreal summer [July–September (JAS)], the decrease in precipitation over the Indian and Asian subcontinent is similar in the model and observations. This suggests that regions of precipitation decrease in response to volcanic forcing move along with seasonal migration of the monsoons and the ITCZ.

Figure 3 shows the 1-yr composite of SAT over land and SST for the model and the observations with CRU SAT over land and HADISSTs over the ocean. In general, the observations show a decrease in temperature over land and ocean in the tropics, with our model results supporting this decrease. We do notice some residual warming in observations over the east Pacific and in the southern Indian Ocean where our ENSO removal technique did not completely remove all the ENSO SST warming during the Agung volcano event as discussed also in the appendix. There is a substantial cooling in the subtropics particularly over the dry arid desert over land both in the model and observations. In these regions, land is seen to cool more than the neighboring oceans due to the lower heat capacity of the land. This difference between the cooling over land and ocean was also seen in Fig. 1 and also in the two panels on the right in Fig. 4, indicating that during major volcanic events, the land–sea contrast in temperature is reduced. One of the caveats of using temperature as a measure of land–sea contrast is that in regions where precipitation decreases local warming is also observed. This is primarily due to two factors: 1) a decrease in cloud cover increases the shortwave radiation reaching the surface and 2) regions with lower precipitation have lower evaporation, which

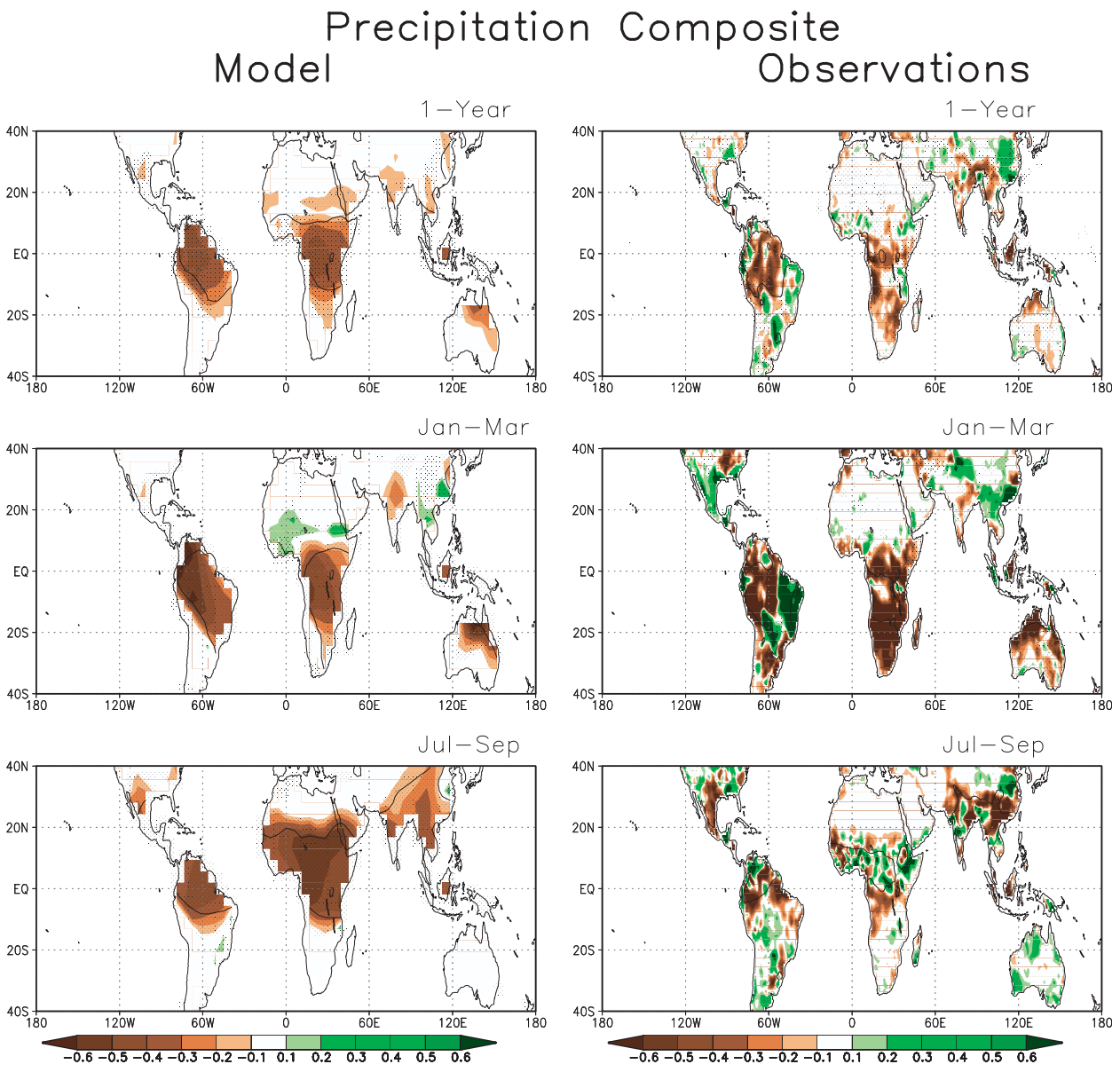

FIG. 2. Composites of precipitation anomalies of the 3 volcanic events for the (left) model and (right) CRU observations for 1 year during the peak response period to volcanic aerosol forcing. (top) The 1-yr-average response and the seasonal migration of precipitation decrease for the (middle) austral and (bottom) boreal summer. Units are in mm day^{-1}. The anomalies from the appropriate seasons of the 3 volcanic events, Pinatubo (peak period: Oct 1991–Sep 1992), El Chichón (peak period: Jul 1982–Jun 1983), and Agung (peak period: Jul 1963/Jun 1964) are averaged to create the composite after the trend is removed. The 5 mm day^{-1} contour of the climatology for the whole period is plotted for reference. Regions significant at the 95% level using the Student's *t* test are indicated as dots in the background.

also leads to a local warming. This is particularly seen in observations where the decrease in climatological precipitation in observations is coupled with a local warming (cf. Figs. 2 and 3). This effect also explains why in the zonally averaged plot of temperature, the equatorial region is warmer than the subtropics even when the aerosol forcing is generally stronger around equator (the two panels on the right in Fig. 4). Nevertheless, the land–sea thermal contrast is clear outside the regions with reduced precipitation such as the large cooling on land over North Africa–Mediterranean and East Asia, seen both in the model and observations. Though not a focus in this paper, the extratropical winter warming discussed in Stenchikov et al. (2004) and Robock (2000) is not captured in our model owing to the lack of a stratosphere. However, the results of the surface temperature response in our model

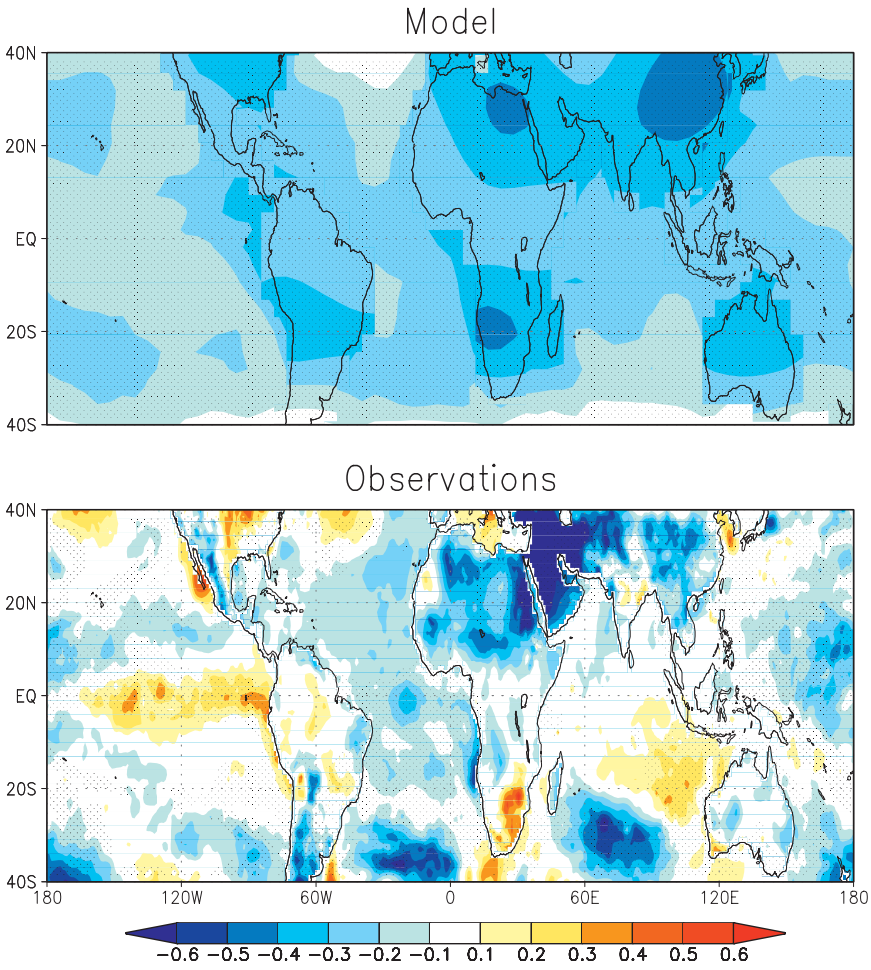

FIG. 3. The 1-yr-averaged spatial temperature response for (top) the 3-event composite in the model, represented by SAT over land and SST over the ocean for the model and (bottom) observations (CRU SAT over land and HadISSTs over the ocean). Units are in K. Composites are calculated as described in Fig. 2. Regions significant at the 95% level using the Student's *t* test are indicated as dots in the background.

are similar to the results of geoengineering experiments in Robock et al. (2008) in which the sulfate aerosols in the stratosphere are well mixed.

The larger cooling over land than the surrounding oceans in the appropriate summer hemisphere might be partly responsible for driving the lower precipitation due to lower land sea–contrast in temperature. This can be further seen in Fig. 4, where the Hovmöller plots of optical depth and the model precipitation and temperature anomalies over land and ocean are presented for the Pinatubo event. The seasonal migration of the precipitation anomalies over land are seen once the zonal mean optical depth has reached 0.02 in the tropics. The region of maximum precipitation indicating the climatological movement of the monsoon and the ITCZ over land is indicated by the 5 mm day^{-1} contour. Approximately a 10% reduction of precipitation over land is noted zonally in the model with a decrease in precipitation lasting for about 3 years. The seasonal migration of precipitation anomalies seems to be supported by a slightly larger cooling over the land than the oceans by about 0.1 K, as was seen in Fig. 1b and Fig. 3. The SST takes longer to cool and this cooling lasts longer and is less strong than the land SAT at the corresponding latitude. Over the ocean, the precipitation anomalies lag that of the ocean by about 6 months, and in our model it is locked to the movement of the ITCZ.

Further support of the seasonal migration of precipitation anomalies over land comes from the comparison of the three volcanic events that erupted at different times of the year. Yet, after the initially staggered response, the precipitation anomalies all get locked into the same

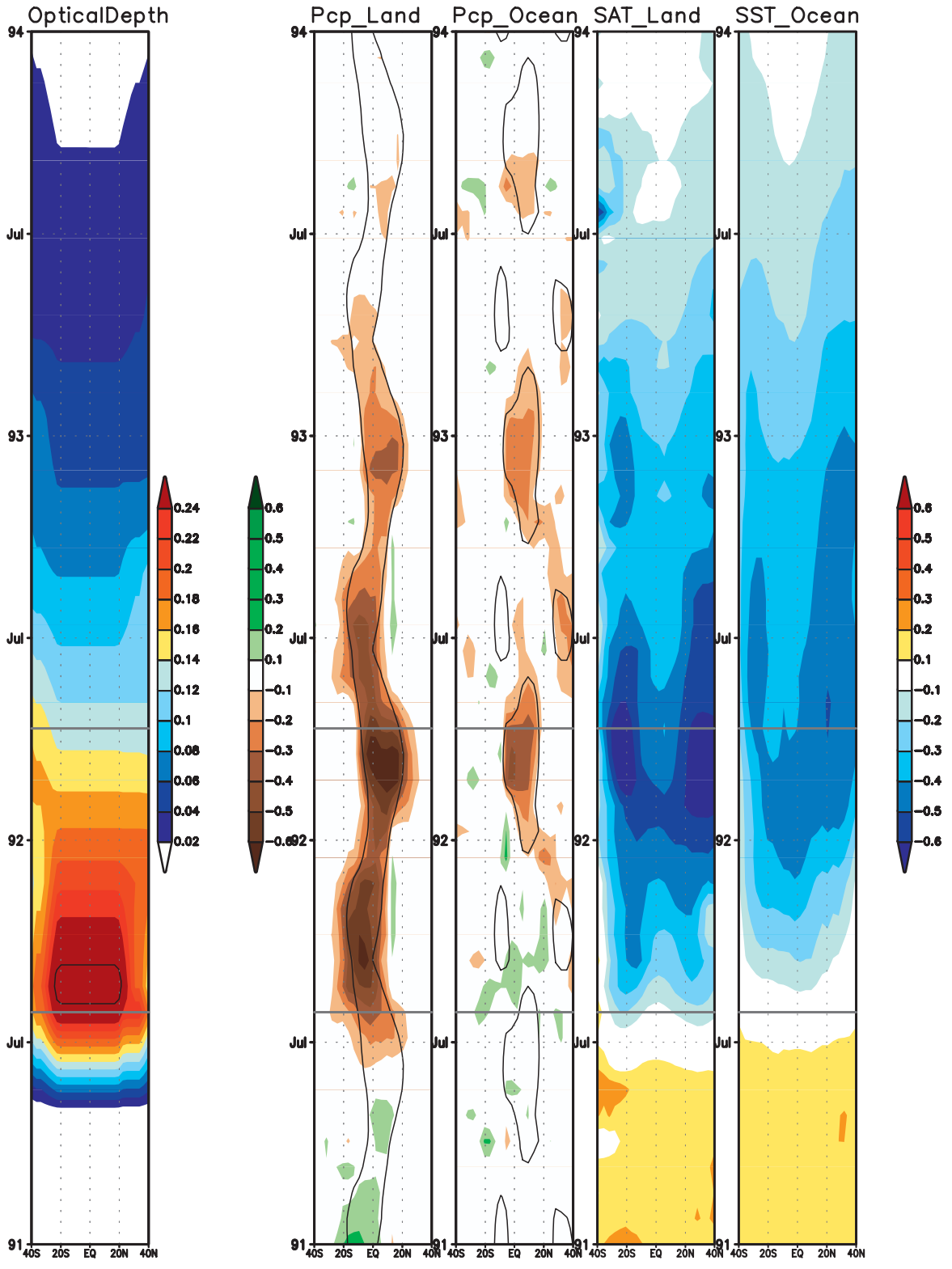

FIG. 4. Hovmöller plots of the model for the Pinatubo event: (left to right) The aerosol optical depth, anomalous precipitation over land and over ocean (mm day^{-1}), and anomalous SAT over land and SST over ocean (K). The anomalies are calculated from the 1981–2000 climatology. The contour for the optical depth is for a value of 0.28, while the contours in precipitation are for the 5 mm day^{-1} climatology. The contour line of precipitation climatology is plotted to indicate the seasonal movement of precipitation.

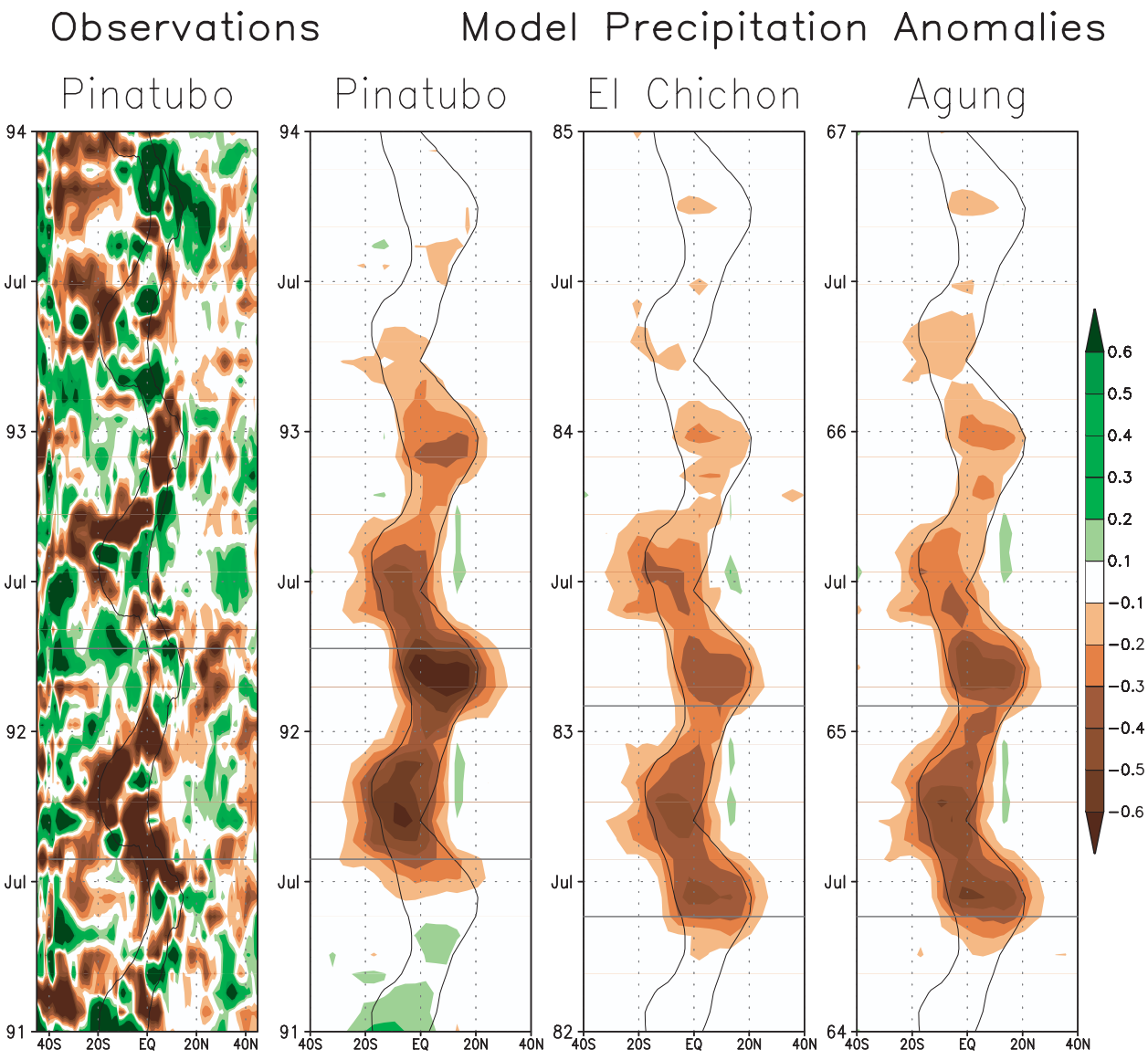

FIG. 5. Hovmöller plots showing the seasonal movement of precipitation anomalies over land for the (left) Pinatubo event from CRU observations; and (left to right) the Pinatubo, El Chichón, and Agung events from the model. The anomalies of Pinatubo and El Chichón are from the 1981–2000 climatology while that of Agung is from 1961–1980 climatology. ENSO is regressed out in the observations as described in the text. Units are in mm day^{-1}. The contours in precipitation are for the 5 mm day^{-1} climatology; and this qualitatively indicates the seasonal movement of precipitation.

seasonal cycle, that is, following the climatological precipitation (Fig. 5). For instance, the optical depth of the El Chichón and Agung volcanoes peaked in July, while that of Pinatubo in November. However, the model responds with a decrease in regions of high precipitation following the movement of the monsoons and the ITCZ in all the cases: the decrease in precipitation lasting between 2 and 3 years. The precipitation anomalies for the CRU observations for the Pinatubo eruption shows a decrease in precipitation in the region of the monsoons and ITCZ (with zonal mean precipitation greater than 5 mm day^{-1}) though the anomalies in the observations are less organized and contain more variability. As discussed earlier the observations of precipitation are less reliable in the earlier periods. The most noticeable decrease in precipitation is in the Southern Hemisphere in the austral summer which is dominated by the decrease in precipitation over the South African monsoon and the Australian monsoon region.

To further understand the decrease in the monsoonal flow, in Fig. 6 we show the total moisture convergence overlaid with vertically integrated moisture transport for

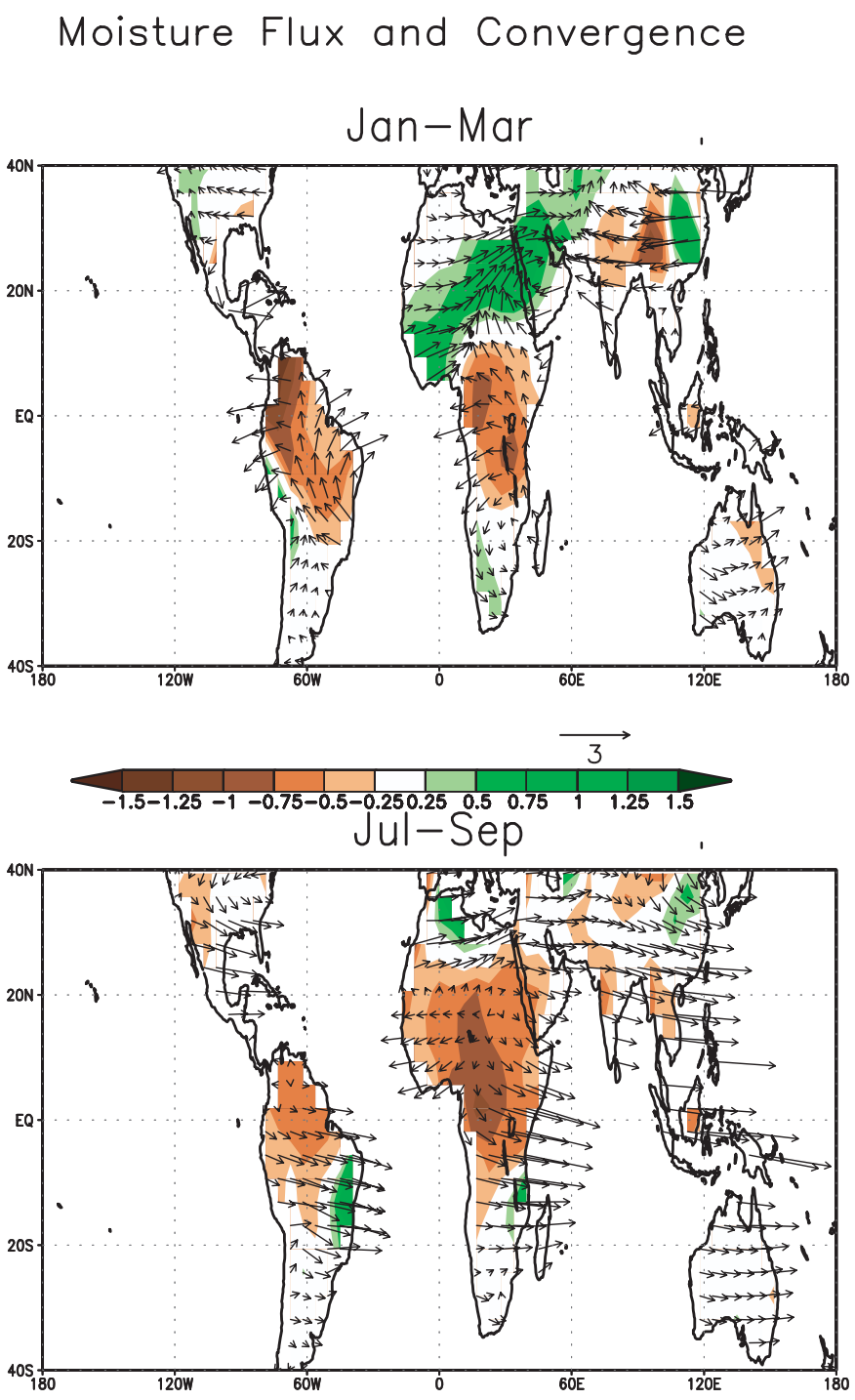

FIG. 6. Composites of vertically integrated moisture convergence (10–6 s^{-1}) overlaid with vertically integrated moisture flux (m s^{-1}) of the 3 volcanic events in the model. The anomalies of Pinatubo and El Chichón are from the 1981–2000 climatology while that of Agung is from 1961–1980 climatology.

the austral and boreal summer periods indicated in Table 1 for the appropriate composites of the model. We note a clear reversal of the wind directions that we would expect during monsoon seasons. The winds of the Australian and the South African monsoon are reversed in the summer austral summer as are those of the East Asian, North American , and East African monsoon in the boreal summer. The vertically integrated moisture convergence

supports this by the decrease in moisture in these regions. This supports the idea that the precipitation decrease over land exists because of a lower moisture convergence which in turn exists due to a smaller land-sea contrast.

The seasonal decrease in anomalous precipitation both in model and observations over land in regions where the total precipitation is a maximum has been shown. This decrease in precipitation is due to the larger decrease in temperature over land compared to the surrounding oceans. This mechanism could drive a weaker monsoonal circulation in the summer seasons of both hemispheres. To further understand the mechanisms and timing of events, we examine the model variables: shortwave radiation reaching the surface, surface air temperature, precipitation, and evaporation change over land and ocean averaged over the region between 40°S and 40°N for the Pinatubo event in Fig. 7. The same analysis has been repeated for the three volcanic events and the results are consistent. Reduction in shortwave radiation at the surface reaches a peak value at 3.5 W m^{-2} 2–3 months after the aerosol optical depth becomes a maximum. The response over land and ocean show dramatic difference, as described below.

To facilitate comparison of the time evolution of events, we use a time marker that corresponds to the first month chosen to represent the Pinatubo eruption (i.e., Oct 1991). Oceanic SST response to Pinatubo is relatively slow, reaching a peak value of approximately −0.3 K after about 1 year of the time marker. Evaporation decrease peaks at 1 month after SST while precipitation lags further by another month. This is consistent with the notion that the relatively large heat capacity of the ocean leads to a delayed response in SST to radiative forcing. This is in turn reduces evaporation and subsequently forces a reduction in precipitation. This mechanism is not unlike the atmospheric response to El Niño SST anomalies.

In contrast, the response of the land is distinctly different. The land precipitation response to the Pinatubo event is rapid and reaches a peak value of about −0.15 mm day^{-1} after about 5 months of the time marker, with evaporation lagging slightly and surface temperature lagging precipitation by about 4 months. This large difference between land and ocean is fundamentally because land has a much lower heat capacity so that the moisture convergence (therefore precipitation) responds quickly to any imbalance in the energy budget. Over the ocean SST acts as a forcing (or at least as an intermediary to propagate heating anomalies to circulation and precipitation changes) leading to evaporation change and then a change in precipitation. However, over land, the chain of response is very different. Surface temperature is a response to land surface water and energy balance and it is the total heating that directly drives moisture convergence and therefore precipitation, while evaporation is a response and feedback, as opposed to be forcing as in the ocean. This happens because of the much lower heat capacity over land. A theoretical framework that details this thinking was presented in Zeng and Neelin (1999). The difference in heat capacity also fundamentally determines the seasonal migration of precipitation anomaly following the climatological precipitation discussed above. These results are consistent with the results of Lambert and Allen (2009) who examined the tropospheric energy budget and concluded that the ocean and land behave differently with respect to radiative perturbations to the energy budget.

A potentially important impact of cooling and reduced precipitation is on ecosystems and carbon cycle. The top panel in Fig. 8 shows the three-event composite of the model-simulated net land-atmosphere carbon flux (F_{ta}) or net ecosystem exchange following the volcanic eruptions. In many of the tropical regions, land atmospheric flux is reduced. Here, two countering mechanisms are at play as indicated in the following equation:

$$F_{ta} = R_h - \mathrm{NPP},$$

where R_h is the heterotrophic respiration (bottom panel of Fig. 8), which describes the carbon released to the atmosphere as a result of temperature-dependent decomposition, and NPP is the net primary production, which is the carbon taken up from the atmosphere due to plant growth (central panel of Fig. 8). To explain the additive nature of R_h and NPP the color scale for NPP is reversed with green indicating a positive flux from the land to the atmosphere. Therefore, on the one hand, drought would reduce vegetation productivity, thus less carbon uptake. On the other hand, the cooling would reduce respiration loss, thus less CO_2 release from the soil. The fact that overall the model simulates a reduction in the net flux indicates that the cooling effect on respiration is stronger than precipitation effect on productivity, consistent with other model studies (Peylin et al. 2005; Zeng et al. 2005). A natural analog has been noted for the after-Pinatubo response of the terrestrial biosphere, although the carbon cycle models have not converged on the relative importance of these processes (Nemani et al. 2003). What is clear is that this cooling and drying is very different from typical ENSO response where warming accompanies drying (Zeng et al. 2005). However, there are two regions (northern Australia and western South America) where NPP response is different from most other regions, indicating the competing effects of cooling and drying on NPP and R_h are such that R_h does not always dominate. We expect such regional features to be highly model and parameterization scheme sensitive.

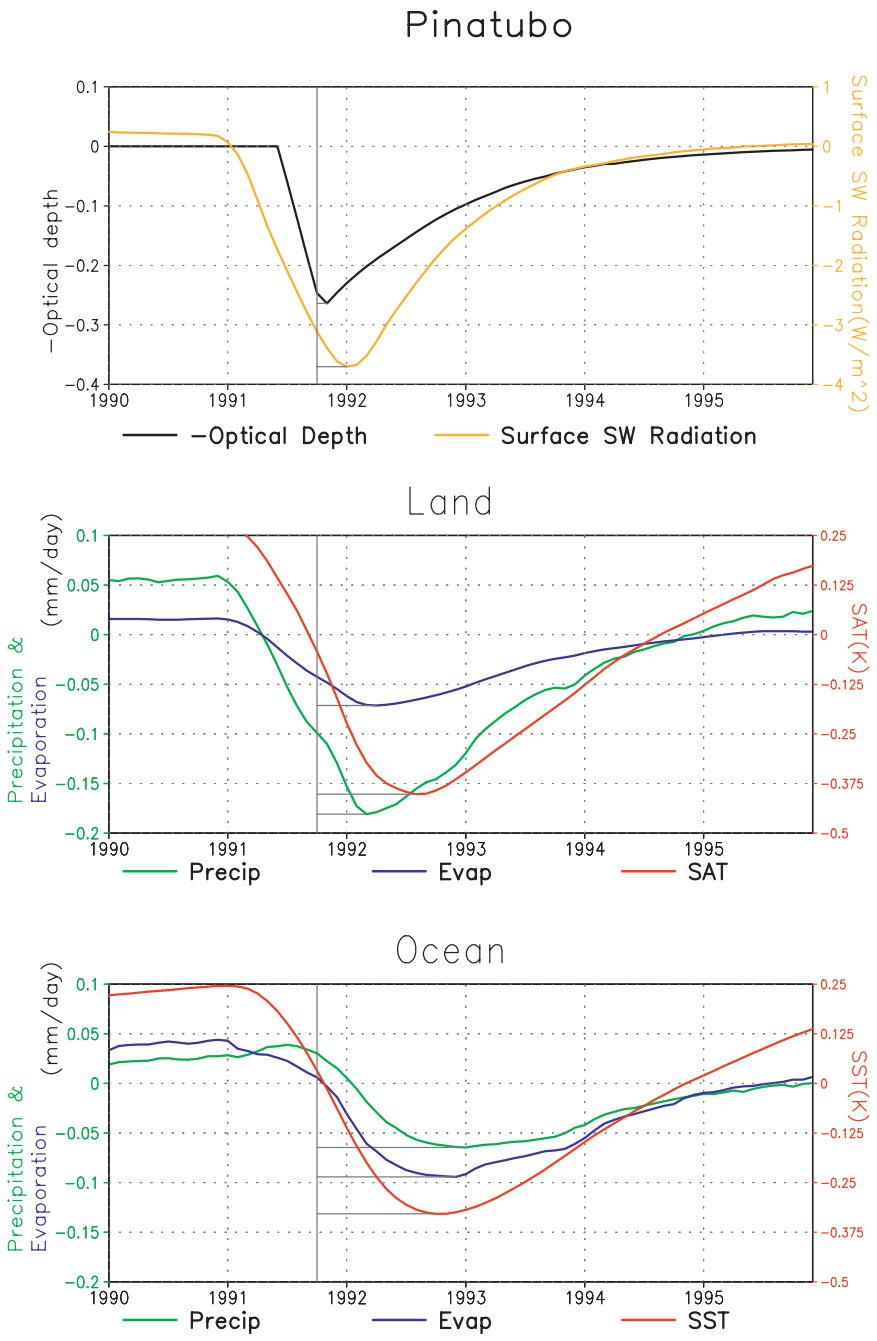

FIG. 7. The response in the model to Pinatubo aerosol forcing: (top) The aerosol optical depth in black used to force model. The response of shortwave radiation at the surface is in light brown. The precipitation response in green, evaporation in blue, and surface air temperature anomaly in red for the (middle) land and (bottom) SSTs for ocean. Units are W m^{-2} for the shortwave radiation; mm day^{-1} for evaporation and precipitation; and K for SAT and SSTs. All lines are smoothed with a 12-month filter. The time marker indicates the first month use for averaging in the study. For Pinatubo it is Oct 1991 (see Table 1).

4. Conclusions

A coupled atmosphere–ocean–land–vegetation model along with observational data is used here to understand the underlying mechanisms of precipitation decrease due to volcanic aerosols. Only the direct effect of the aerosols contributing to the reduction in shortwave radiation is examined here. An advantage of the particular model

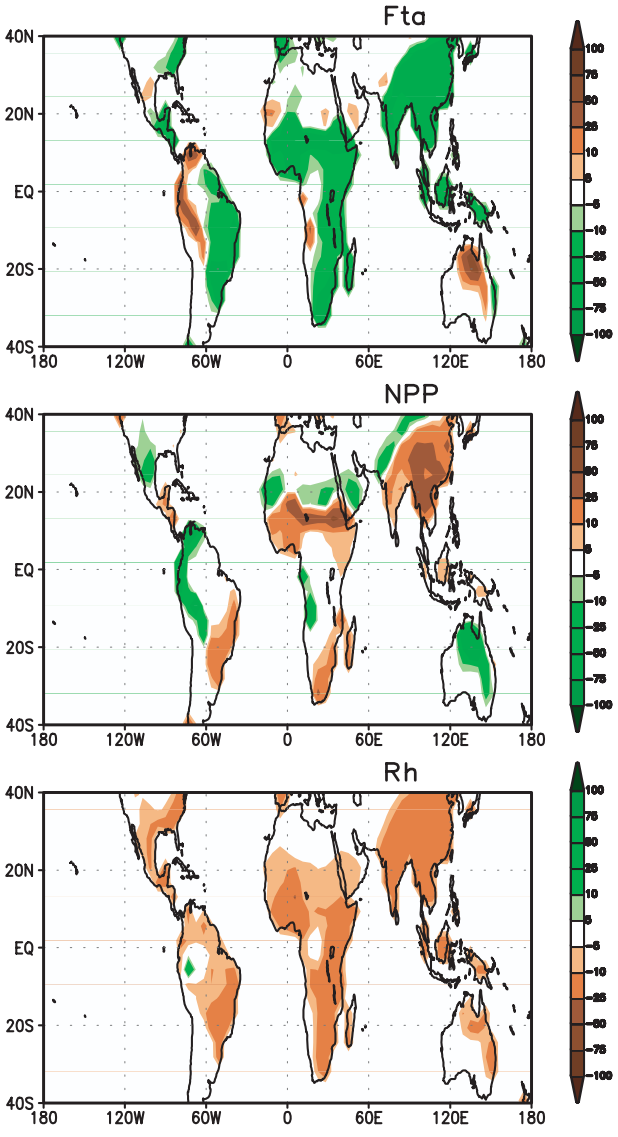

FIG. 8. The 3-event composite response of the land–atmosphere carbon flux (F_{ta}), net primary production (NPP), heterotrophic respiration (R_h) in gC m^{-2} yr^{-1} for the 1-yr period indicated in the text. The shading for NPP is opposite to R_h and F_{ta}.

employed is that the variability from interannual to interdecadal scales is minimized because of the use of a mixed layer model for the ocean. Hence, the volcanic signals are not masked by climatic effects dependent on more complicated dynamics (i.e., ENSO). On the other hand, many processes have been simplified, limiting any interaction feeding back onto any oceanic dynamics. Nevertheless, our model captures the right magnitude of the temperature (~0.35 K) and precipitation (~0.15 mm day^{-1}) decrease for the region of 40°N–40°S as compared to observations. The agreement is particularly good for the Pinatubo event where the precipitation data is also most reliable.

Complementing existing studies on the precipitation response to volcanic aerosol, we highlight a clear seasonal migration of the rainfall anomalies that follows the climatological monsoons over land. We hypothesize two reasons for this phase locking. First, precipitation responds with a 4–5-month time scale over land owing to the energy imbalance caused by volcanic aerosol cooling, similar to the response after the thermal peak of an ENSO event (e.g., Qian et al. 2008). In contrast, the precipitation response over oceans is much slower (~1 year) and is considerably damped because of the much larger heat capacity. The difference in heat capacities over land and over ocean additionally leads to an anomalous land–sea thermal heat contrast, which could further contribute to the reduction in rainfall over land via reduction of monsoonal flows.

The model responses to the exogenous forcing are clearly very different over land and ocean. Over the ocean, SST responds to volcanic forcing, followed by evaporation and then precipitation. In contrast, land precipitation responds quickly to the forcing, followed by evaporation, with surface temperature responding slowest. The surface energy and water balances are clearly different over land and ocean, and further study on the details of the hydrological cycle under volcanic aerosol forcing is warranted.

The dynamical vegetation model responds to volcano-induced drought and cooling, showing an anomalous carbon uptake of 50–100 gC m^{-2} yr^{-1} over many tropical and subtropical region. Our results are consistent with several previous studies in that the reduction in the net carbon flux to the atmosphere indicates that the cooling effect on respiration is stronger than precipitation effect on productivity (Peylin et al. 2005; Zeng et al. 2005; Gu et al. 2002; Jones and Cox 2001). This has significant implication for the ecosystem, agriculture, and the carbon cycle especially in the monsoon regions.

The cooling effects of volcanoes due to high loadings of stratospheric aerosol have been well known for over a century. However, the impact on precipitation has only recently been stressed. This paper has emphasized the seasonal varying nature of the reduction in precipitation due to the direct effects of volcanic aerosols, in particular focusing on the seasonally locked nature of the induced tropical–subtropical drought of three large late twentieth-century eruptions. Also highlighted are the differences in mechanisms that could lead to the reduction in precipitation over land and over ocean as seen in the QTCM, a model of intermediate complexity. The reduction in precipitation and the cooling of the earth system both have been shown to have important implications for the ecosystem and carbon cycle over the tropics. This research provides a glimpse of the impact that stratospheric aerosol geoengineering could have on the hydrological cycle.

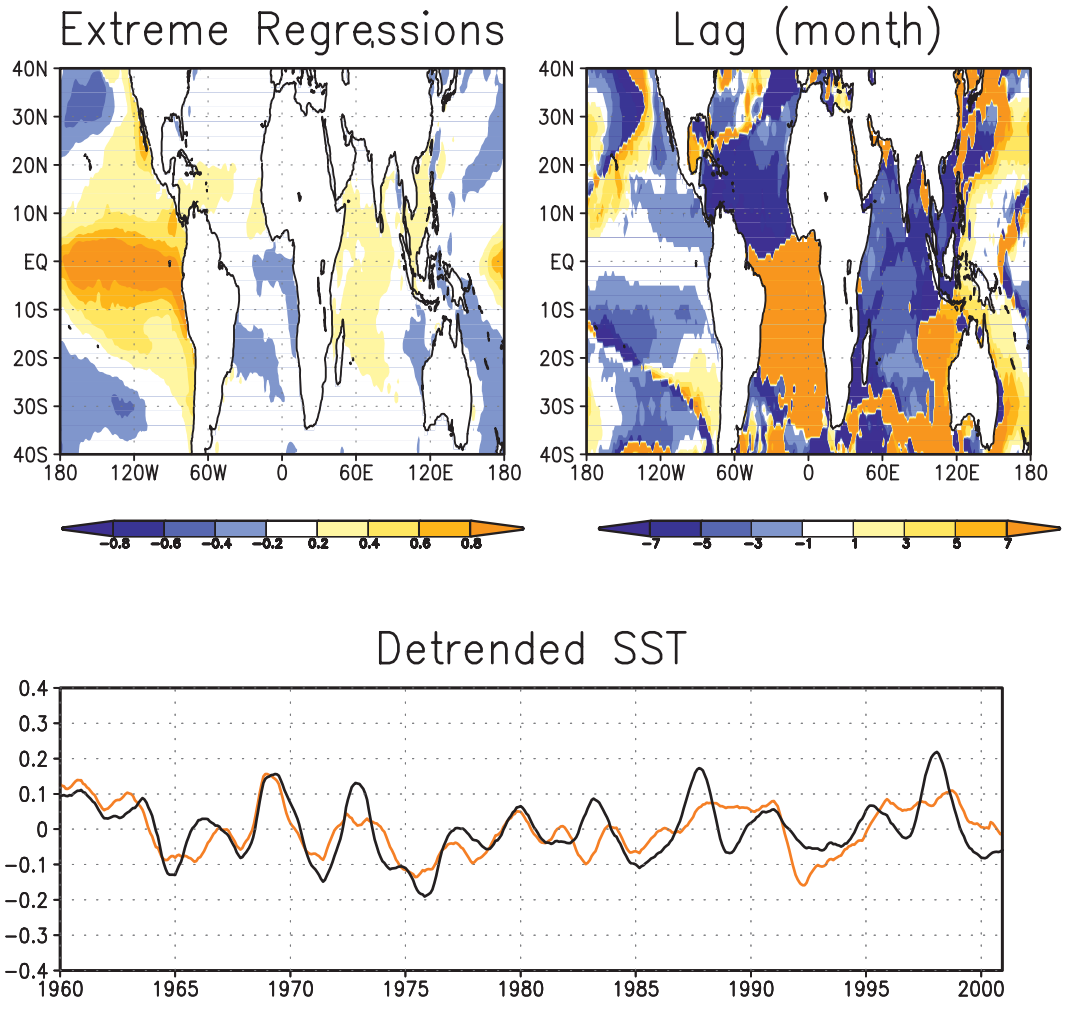

FIG. A1. (top left) The values in K at every latitude–longitude point corresponding to largest regressions of HadISST data with the Niño-3.4 index obtained within a 12-month lead–lag window. (top right) The corresponding lag in months at which those values are largest. The top two figures bear a strong resemblance with those of Chen et al. 2008 (their Fig. A2). (bottom) The detrended HADISST data averaged between 40°N and 40°S in black and corresponding data with ENSO removed in orange as explained in the appendix.

Acknowledgments. We thank J-H. Yoon for providing the model simulation results. We also thank the four anonymous reviewers for their valuable comments, which have helped enhance the quality of this paper. This research was supported by NSF Grant ATM0739677, NOAA Grants NA17EC1483, NA04OAR4310091, and NA04OAR4310114, and NASA Grant 407191AG7.

APPENDIX

Removal of ENSO

ENSO is known to affect different regions through teleconnections at different lags. Hence, removal of the effects of contemporaneous correlations–regressions is not necessarily effective in removing the maximum impact of ENSO. The method used to remove ENSO in this paper is similar to that of Chen et al. (2008). With the intent of removing the maximum impact of ENSO over each grid point, regressions–correlations with the Niño-3.4 index with a lag of up to 12 months are first calculated. Then the month of the most extreme lag correlation for each spatial point is used to calculate regressions with lag to that month. The regressed values are then removed from the observations. It is worth noting that using the month of extreme correlations, as in Chen et al. (2008), or using the month of extreme regressions (as in this paper) to calculate the lag regressions produces similar results.

An illustration of the method is indicated in Fig. A1 for the HadISST data. The top-right panel shows the month in which extreme regressions occurred, while the top-left

panel shows the extreme regressions that occur at the respective lags indicated in the top-right panel. These two panels are similar to Fig. A2 in Chen et al. (2008), except that their study used surface temperature from the International Comprehensive Ocean–Atmosphere Dataset (ICOADS) and extreme correlations to remove ENSO, while the results shown here use HadISSTs and extreme regressions over the ocean to remove ENSO. Extreme positive regressions are observed in the central and eastern Pacific with 0 lag. This is the region most affected by ENSO. The eastern Pacific off the California coast and the coast of Chile also has positive values of regression; these values correspond to a lag and lead of about three months, respectively. The lag along the eastern Pacific off the California coast is well known (Rasmusson and Carpenter 1982), while the lead along the Chilean coast can be attributed to the weaker trade winds that lead the ENSO SST event. Regressions are maximized in the Indian Ocean with a lag of 3–5 months. This can be attributed to increased subsidence and a decrease in monsoon activity and cloudiness (e.g., Lau and Yang 1996). Not all the features corresponding to the lead–lag relationship can be simply understood, though the relationships recovered by our method bear close correspondence to the results in Chen et al. (2008). The bottom panel in Fig. A1 shows the result of the detrended data with and without the removal of ENSO. This clearly shows that our technique is capable of removing strong ENSO events toward the latter 30 years of the last century. However, some of the earlier events prior to the climate shift in ENSO climate in the 1970s are not clearly removed. This does not negatively impact the results of the paper based on the simulation because the model has no ENSO.

REFERENCES

Adler, R. F., and Coauthors, 2003: The Version-2 Global Precipitation Climatology Project (GPCP) monthly precipitation analysis (1979–present). *J. Hydrometeor.,* **4,** 1147–1167.

Amman, C. M., G. A. Meehl, W. M. Washington, and C. S. Zender, 2003: A monthly and latitudinally varying volcanic forcing dataset in simulations of 20th century climate. *Geophys. Res. Lett.,* **30,** 1657, doi:10.1029/2003GL016875.

Bala, G., P. B. Duffy, and K. E. Taylor, 2008: Impact of geoengineering schemes on the global hydrological cycle. *Proc. Natl. Acad. Sci. USA,* **105,** 7664–7669, doi:10.1073/pnas.0711648105.

Chen, J., and Coauthors, 2008: The spatiotemporal structure of twentieth-century climate variations in observations and reanalyses. Part I: Long-term trend. *J. Climate,* **21,** 2611.

Compo, G. P., and P. D. Sardeshmukh, 2010: Removing ENSO-related variations from the climate record. *J. Climate,* **23,** 1957–1978.

Crowley, T. J., 2000: Causes of climate change over the past 1000 years. *Science,* **289,** 270–277.

Franklin, B., 1784: Meteorological imaginations and conjectures. *Mem. Proc. Lit. Philos. Soc.,* **2,** 357–361.

Free, M., and J. K. Angell, 2002: Effect of volcanoes on the vertical temperature profile in radiosonde data. *J. Geophys. Res.,* **107,** 4101, doi:10.1029/2001JD001128.

Friedlingstein, P., and Coauthors, 2006: Climate–carbon cycle feedback analysis: Results from the C4MIP model intercomparison. *J. Climate,* **19,** 3337–3353.

Gu, G., R. F. Adler, G. J. Huffman, and S. Curtis, 2007: Tropical rainfall variability on interannual-to-interdecadal/longer-time scales derived from the GPCP monthly product. *J. Climate,* **20,** 4033–4046.

Gu, L., D. Baldocchi, S. B. Verma, T. A. Black, T. Vesala, E. M. Falge, and P. R. Dowty, 2002: Advantages of diffuse radiation for terrestrial ecosystem productivity. *J. Geophys. Res.,* **107,** 4050, doi:10.1029/2001JD001242.

Hansen, J., A. Lacis, D. Rind, G. Russell, P. Stone, I. Fung, R. Ruedy, and J. Lerner, 1983: Climate sensitivity: Analysis of feedback mechanisms in climate processes and climate sensitivity. *Climate Processes and Climate Sensitivity, Geophys. Monogr.,* Vol. 29, Amer. Geophys. Union, 130–163.

——, ——, R. Ruedy, and M. Sato, 1992: Potential climate impact of Mount Pinatubo eruption. *Geophys. Res. Lett.,* **19,** 215–218.

Huffman, G. J., and Coauthors, 1997: The Global Precipitation Climatology Project (GPCP) combined precipitation dataset. *Bull. Amer. Meteor. Soc.,* **78,** 5–20.

Humphreys, W. J., 1940: *Physics of the Air*. Dover, 676 pp.

Jones, C. D., and P. M. Cox, 2001: Modeling the volcanic signal in the atmospheric CO_2 record. *Global Biogeochem. Cycles,* **15,** 453–465.

Jones, P. D., A. Moberg, T. J. Osborn, and K. R. Briffa, 2003: Surface climate responses to explosive volcanic eruptions seen in long European temperature records and mid-to-high latitude tree-ring density around the Northern Hemisphere. *Volcanism and the Earth's Atmosphere, Geophys. Monogr.,* Vol. 139, Amer. Geophys. Union, 239–254.

Koch, D., D. Jacob, I. Tegen, D. Rind, and M. Chin, 1999: Tropospheric sulfur simulation and sulfate direct radiative forcing in the Goddard Institute for Space Studies general circulation model. *J. Geophys. Res.,* **104,** 23 799–23 822.

Kucharski, A., and Coauthors, 2008: The CLIVAR C20C project: Skill of simulating Indian monsoon rainfall on interannual to decadal timescales. Does GHG forcing play a role? *Climate Dyn.,* **33,** 615–627, doi:10.1007/s00382-008-0462-y.

Lambert, F., and M. R. Allen, 2009: Are changes in global precipitation constrained by the tropospheric energy budget? *J. Climate,* **22,** 499–517.

Lau, K.-M., and S. Yang, 1996: The Asian monsoon and predictability of the tropical ocean–atmosphere system. *Quart. J. Roy. Meteor. Soc.,* **122,** 945–957.

Levitus, S., J. I. Antonov, T. P. Boyer, and C. Stephens, 2000: Warming of the world ocean. *Science,* **287,** 2225–2229.

Minnis, P., E. F. Harrison, L. L. Stowe, G. G. Gibson, F. M. Denn, D. R. Doelling, and W. L. Smith Jr., 1993: Radiative climate forcing by the Mt. Pinatubo eruption. *Science,* **259,** 1411–1415.

Mitchell, T. D., T. R. Carter, P. D. Jones, M. Hulme, and M. New, cited 2004: A comprehensive set of high-resolution grids of monthly climate for Europe and the globe: The observed record (1901–2000) and 16 scenarios (2001–2100). Tyndall Centre for Climate Change Research, Working Paper 55. [Avaiable online at http://www.tyndall.ac.uk/sites/default/files/wp55.pdf.]

Neelin, J. D., and N. Zeng, 2000: A quasi-equilibrium tropical circulation model—Formulation. *J. Atmos. Sci.,* **57,** 1741–1766.

Nemani, R. R., and Coauthors, 2003: Climate-driven increases in global terrestrial net primary production from 1982 to 1999. *Science,* **300,** 1560–1563.

Oman, L., A. Robock, G. Stenchikov, G. A. Schmidt, and R. Ruedy, 2005: Climatic response to high latitude volcanic eruptions. *J. Geophys. Res.,* **110,** D13103, doi:10.1029/2004JD005487.

Penland, C., and L. Matrosova, 2006: Studies of El Niño and interdecadal variability in tropical sea surface temperatures using a nonnormal filter. *J. Climate,* **19,** 5796–5815.

Peylin, P., and Coauthors, 2005: Multiple constraints on regional CO2 flux variations over land and oceans. *Global Biogeochem. Cycles,* **19,** GB1011, doi:10.1029/2003GB002214.

Qian, H., R. Joseph, and N. Zeng, 2008: Response of the terrestrial carbon cycle to the El Niño–Southern Oscillation. *Tellus,* **60,** 537–550, doi:10.1111/j.1600-0889.2008.00360.x.

——, ——, and ——, 2010: Enhanced terrestrial carbon uptake in the northern high latitudes in the 21st century from the C4MIP model projections. *Global Change Biol.,* **16,** 641–656.

Rasch, P. J., S. Tilmes, R. P. Turco, A. Robock, L. Oman, C.-C. Chen, G. L. Stenchikov, and R. R. Garcia, 2008: An overview of geoengineering of climate using stratospheric sulfate aerosols. *Philos. Trans. Roy. Soc.,* **366,** 4007–4037.

Rasmusson, E. M., and T. H. Carpenter, 1982: Variations in tropical sea surface temperature and surface wind fields associated with the Southern Oscillation/El Niño. *Mon. Wea. Rev.,* **110,** 354–384.

Rayner, N. A., D. E. Parker, E. B. Horton, C. K. Folland, L. V. Alexander, D. P. Rowell, E. C. Kent, and A. Kaplan, 2003: Globally complete analyses of sea surface temperature, sea ice and night marine air temperature, 1871–2000. *J. Geophys. Res.,* **108,** 4407, doi:10.1029/2002JD002670.

Robock, A., 2000: Volcanic eruptions and climate. *Rev. Geophys.,* **38,** 191–219.

——, and Y. Liu, 1994: The volcanic signal in Goddard Institute for Space Studies three-dimensional model simulations. *J. Climate,* **7,** 44–55.

——, and J. Mao, 1995: The volcanic signal in surface temperature observations. *J. Climate,* **8,** 1086–1103.

——, L. Oman, and G. L. Stenchikov, 2008: Regional climate responses to geoengineering with tropical and Arctic SO_2 injections. *J. Geophys. Res.,* **113,** D16101, doi:10.1029/2008JD010050.

Scaife, A. A., and Coauthors, 2008: The CLIVAR C20C project: Selected 20th century climate events. *Climate Dyn.,* **33,** 603–614, doi:10.1007/s00382-008-0451-1.

Schneider, D. P., C. M. Ammann, B. L. Otto-Bliesner, and D. S. Kaufman, 2009: Climate response to large, high-latitude and low-latitude volcanic eruptions in the Community Climate System Model. *J. Geophys. Res.,* **114,** D15101, doi:10.1029/2008JD011222.

Soden, B. J., R. T. Wetherald, G. L. Stenchikov, and A. Robock, 2002: Global cooling following the eruption of Mt. Pinatubo: A test of climate feedback by water vapor. *Science,* **296,** 727–730.

Stenchikov, G., K. Hamilton, A. Robock, V. Ramaswamy, and M. D. Schwarzkopf, 2004: Arctic oscillation response to the 1991 Pinatubo eruption in the SKYHI general circulation model with a realistic quasibiennial oscillation. *J. Geophys. Res.,* **109,** D03112, doi:10.1029/2003JD003699.

Trenberth, K. E., and A. Dai, 2007: Effects of Mount Pinatubo volcanic eruption on the hydrological cycle as an analog of geoengineering. *Geophys. Res. Lett.,* **34,** L15702, doi:10.1029/2007GL030524.

Wigley, T. M. L., 2000: ENSO, volcanoes, and record-breaking temperatures. *Geophys. Res. Lett.,* **27,** 4101–4104.

Wild, M., J. Grieser, and C. Schär, 2008: Combined surface solar brightening and increasing greenhouse effect support recent intensification of the global land-based hydrological cycle. *Geophys. Res. Lett.,* **35,** L17706, doi:10.1029/2008GL034842.

Yang, F., A. Kumar, M. E. Schlesinger, and W. Wang, 2003: Intensity of hydrological cycles in warmer climates. *J. Climate,* **16,** 2419.

Zeng, N., 2003: Glacial-interglacial atmospheric CO_2 changes: The glacial burial hypothesis. *Adv. Atmos. Sci.,* **20,** 677–693.

——, and J. D. Neelin, 1999: A land–atmosphere interaction theory for the tropical deforestation problem. *J. Climate,* **12,** 857–872.

——, ——, and C. Chou, 2000: The first quasi-equilibrium tropical circulation model-implementation and simulation. *J. Atmos. Sci.,* **57,** 1767–1796.

——, H. Qian, E. Munoz, and R. Iacono, 2004: How strong is carbon cycle-climate feedback under global warming? *Geophys. Res. Lett.,* **31,** L20203, doi:10.1029/2004GL020904.

——, A. Mariotti, and P. Wetzel, 2005: Terrestrial mechanisms of interannual CO_2 variability. *Global Biogeochem. Cycles,* **19,** GB1016, doi:10.1029/2004GB002273.

Zhou, T., and Coauthors, 2008: The CLIVAR C20C project. Part 3: Which components of the Asian–Australian Monsoon variability are forced and reproducible? *Climate Dyn.,* **33,** 1051–1068, doi:10.1007/s00382-008-0501-8.